International Journal of Astrobiology 12 (2): 135–143 (2013)
doi:10.1017/S147355041200050X

Interaction of forsterite-91 with distilled water and artificial seawater: a prebiotic chemistry experiment

Cláudio M. D. de Souza[1], Cristine E. A. Carneiro[1], João Paulo T. Baú[1], Antonio C. S. da Costa[2], Flávio F. Ivashita[3], Andrea Paesano Jr[3], Eduardo di Mauro[4], Henrique de Santana[1], Nils G. Holm[5], Anna Neubeck[5], Cássia T. B. V. Zaia[6] and Dimas A. M. Zaia[1]

[1]*Laboratório de Química Prebiótica, Departamento de Química-CCE, Universidade Estadual de Londrina, 86051-990 Londrina, PR, Brazil*
e-mail: damzaia@uel.br
[2]*Departamento de Agronomia-CCA, Universidade Estadual de Maringá, 87020-900 Maringá, PR, Brazil*
[3]*Departamento de Física-CCE, Universidade Estadual de Maringá, 87020-900 Maringá, PR, Brazil*
[4]*Laboratório de Fluorescência e Ressonância Paramagnética Eletrônica (LAFLURPE)-CCE, Universidade Estadual de Londrina, 86051-990 Londrina, PR, Brazil*
[5]*Department of Geological Sciences, Stockholm University, Stockholm, Sweden*
[6]*Departamento de Ciências Fisiológicas-CCB, Universidade Estadual de Londrina, 86051-990 Londrina, PR, Brazil*

Abstract: In the present work, the interactions between forsterite-91 with distilled water and forsterite-91 with artificial seawater were studied at two pHs (2.0 and 8.0) using different techniques. A large increase in pH was observed for samples incubated at an initially acidic pH (2.0) due to the dissolution of forsterite-91 in distilled water and artificial seawater. Thus, in acidic hydrothermal vents, an increase in the amount of hydrocarbons and magnetite should be expected due to the release of Fe(II). The pH_{PZC} decreased and the pH_{IEP} increased when forsterite-91 was treated with distilled water and artificial seawater. The ions from the artificial seawater had an effect on zeta potential. Scanning electron microscopy (SEM) images and X-ray diffractograms showed halite in the samples of forsterite-91 mixed with artificial seawater. The presence of halite or adsorption of ions on the surface of forsterite-91 could affect the synthesis of magnetite and hydrocarbons in hydrothermal vents, due to a decrease in the dissolution rates of forsterite-91. The dissolution of forsterite-91 yields low concentrations of Fe(III) and Mn(II) as detected by electron paramagnetic resonance (EPR) spectroscopy. Microanalysis of forsterite-91 showed a higher amount of Mn, with an oxidation that was likely not +II, as Mn in supernatant solutions was only detected by EPR spectroscopy after mixing with artificial seawater at pH 2.0. As Fe(III) and Mn(II) are catalyst constituents of magnetite and manganese oxide, respectively, their presence is important for synthesis in hydrothermal vents. Etch pits were observed only in the forsterite-91 sample mixed with distilled water at pH 8.0. Na, Cl, S, Ca and K were detected in the samples mixed with artificial seawater by SEM–EDS. Si, Mg, Fe and Al were detected in almost all supernatant samples due to forsterite-91 dissolution. Cr was not dissolved in the experiments, thus Cr in the mineral could serve as an effective catalyst for Fischer Tropsch Types (FTT) reactions in hydrothermal vent systems. X-ray diffractograms of the original forsterite-91 also showed peaks arising from zeolites and clinochlore. After the samples were treated with artificial seawater, X-ray diffractograms showed the dissolution of zeolite. Experiments should be performed in the natural environment to verify the potential for zeolites to act as a catalyst in hydrothermal vents.

Received 17 August 2012, accepted 10 December 2012, first published online 7 February 2013

Key words: forsterite-91, olivine, prebiotic chemistry, seawater.

Introduction

A.G. Werner named the mineral olivine in 1790 due to its olive-green color, nowadays this name is used for a group of minerals that form a solid solution with the chemical composition $Fe_{1-x}Mg_xSiO_4$. In 1824, A. Levy named forsterite for the Mg-rich end member of the solid solution, to honour J.R. Forster (1739–1806), an English mineral collector and dealer. In 1840, J.F. Gemelin named fayalite for the Fe end member of the solid solution, after the Island of Faial (Fayal) in the Azores. Therefore, these names and the mol percentage of Fe and Mg in olivine designate precisely the mineral compositions; thus forsterite-91 is the same as fayalite-9 (King 2009).

The most easily accessible source of energy in the lithosphere of any terrestrial planet is the molecular hydrogen that is formed during oxidation of Fe(II) inherent in minerals (Martin *et al*. 2008; Neubeck *et al*. 2011). Olivine formed under high temperature is rich in Fe(II) and Mg, and has very a high dissolution rate compared with other primary minerals. According to Hazen *et al*. (2008), the olivine group of minerals

was one of 60 minerals that formed the Earth. Therefore, the interaction of these primary minerals with the environment of the primitive Earth (atmosphere, light and water) is an important issue for prebiotic chemistry. It should also be pointed out that there are few studies on prebiotic chemistry using olivine (Zaia 2012).

Olivine plays an important role in hydrothermal vents, the geochemical process is known as serpentinization. Under hydrothermal vents conditions, Fe(II) in the rocks reduces H_2O to produce Fe(III), H_2 and hydrocarbons according to the equation below (Martin *et al.* 2008):

$$(Mg, Fe)_2SiO_4 + H_2O + C \rightarrow Mg_3SiO_5(OH)_4 + Mg(OH)_2 + Fe_3O_4 + H_2 + CH_4 + C_2 - C_5.$$

Several authors also showed that olivine dissolution at low temperatures could be linked to the production of H_2/CH_4 (Hellevang 2008; Hellevang *et al.* 2011; Neubeck *et al.* 2011).

The dissolution of olivine was studied under several different conditions. According to Nahon *et al.* (1982) weathering of olivine under humid tropical conditions produces successively: smectite, amorphous oxyhydroxides rich in silica and well-crystallized oxyhydroxides. This sequence is associated with the continuous leaching of calcium, magnesium, silica and oxidation of the Fe(II) to Fe(III) from the parent rock. Gíslason & Arnósson (1993) studied the dissolution of olivine in various types of natural water (river water, groundwater and geothermal waters) in Iceland. According to these authors, the stability of olivine decreases with increasing Mg content. Giammar *et al.* (2005) observed that forsterite dissolution increased with increasing temperature and P_{CO2}. Stopar *et al.* (2006) observed that the dissolution of olivine with fayalite-rich compositions was favoured for small particle sizes, at acidic pH and at high temperatures. Olsen & Rimstidt (2008) showed that forsterite dissolution depends on the pH and the concentration of oxalate.

In the present work, the dissolution of forsterite-91 was studied at two different pHs (2.0 and 8.0) in distilled water and artificial seawater. These pHs were chosen to emulate the acidic and basic pHs that have been observed in hydrothermal vent fluids (black smokers, LCHF-Lost City Hydrothermal Fields) (Martin *et al.* 2008). It should be noted that hydrothermal environments are still present on Earth today and were probably more common on prebiotic Earth (Martin *et al.* 2008). Acidic lakes are also common on Earth and they can be used as models of Martian lakes (Mormile *et al.* 2009). The composition of salts and their concentration in the seawater of the prebiotic Earth are controversial issues (Zaia 2012); thus, the artificial seawater used for this study contained all major elements. After the interaction of forsterite-91 with distilled water or artificial seawater, the samples were analysed using several spectroscopic methods (Fourier Transform Infrared (FT-IR), electron paramagnetic resonance (EPR), Raman and Mössbauer), zeta potential, scanning electron microscopy (SEM), Scanning electron microscopy-Energy Dispersive X-ray Spectroscopy (SEM-EDS) and X-ray diffractometry. It also should be pointed out that, as far as we know, no studies have investigated the interaction between forsterite-91 and artificial seawater using all of the above-mentioned methods and under conditions that mimic the prebiotic Earth.

Table 1. *Chemical composition of forsterite-91*

Substance	Amount	Method
Total solids (TS)	99.9%	Wet chemistry
SiO_2	41.2 ± 3.3%	ICP-AES[a]
Al_2O_3	0.213 ± 0.019%	ICP-AES[a]
CaO	< 0.09%	ICP-AES[a]
Fe_2O_3	9.03 ± 0.72%	ICP-AES[a]
K_2O	< 0.1%	ICP-AES[a]
MgO	52.1 ± 4.1%	ICP-AES[a]
MnO	0.111 ± 0.011%	ICP-AES[a]
Na_2O	< 0.06%	ICP-AES[a]
P_2O_5	< 0.01%	ICP-AES[a]
TiO_2	0.0027 ± 0.0002%	ICP-AES[a]
Sum	102.7%	
Cr	1620 ± 217 mg kg^{-1}	ICP-AES[a]
Ni	3010 ± 733 mg kg^{-1}	ICP-SFMS[b]

[a] Inductively coupled plasma atomic emission spectroscopy.
[b] Inductively coupled plasma sector field mass spectrometer.

Materials and methods

Materials

All reagents were of analytical grade (P.A). Table 1 shows analysis of forsterite-91.

Seawater

The following substances were weighed and dissolved in 1.0 L of distilled water: 28.57 g of sodium chloride, 3.88 g of magnesium chloride, 1.787 g of magnesium sulphate, 1.308 g of calcium sulphate, 0.832 g of potassium sulphate, 0.103 g of potassium bromide and 0.0282 g of boric acid (Brown *et al.* 2004; Zaia 2012).

Forsterite manipulation

Natural olivine sand (Forsterite-91, Fo91) was obtained from North Cape Minerals in Åheim, Norway. The original sample was gently ground in an agate mortar, all materials passing through a 53 mesh sieve were saved in plastic vials for further analyses.

Samples preparation

To two different sets of duplicate tubes (15 mL) each containing 100 mg of forsterite-91 were added 5.00 mL of distilled water and 5.00 mL of artificial seawater. The pHs were adjusted with HCl (1.0 mol L^{-1}) or NaOH (1.0 mol L^{-1}) until they reached the ranges 1.9–2.2 and 8.0–8.4. The contents in the tubes were mixed for 24 hours and spun for 15 minutes at 2000 rpm. The aqueous phase and the solid phase of the samples were lyophilized. The lyophilized aqueous phase was used for EPR spectroscopy and SEM-EDS determinations. The lyophilized solid samples were used for pH_{PZC}, zeta

https://doi.org/10.1017/S147355041200050X Published online by Cambridge University Press

potential, FT-IR, Raman, EPR, Mössbauer spectroscopy, X-ray diffractometry and scanning electron microscopy.

Methods

Determination of pH_{PZC}

We used 1.00 g of forsterite-91/2.5 mL (1.0 mol L^{-1} KCl or distilled water) ratio. The pH at the point of zero charge was calculated using the equation: $pH_{PZC} = 2\,pH$ (1.0 mol L^{-1} KCl) – pH (distilled water) (Uehara 1979).

Zeta potential (ζ)

A Zetaplus Analyzer (Zetaplus, Brookhaven, NY, USA) was used to measure the zeta potentials of forsterite-91's samples at 25 ± 1 °C. Samples of forsterite-91 were suspended in aqueous solution (0.01 wt%). The ionic strength was maintained using a solution of 10^{-3} mol L^{-1} KCl (pH 1.9–11.4). The pH isoelectric point (pH_{IEP}) was determined graphically (Zeta-Potential versus pH).

Infrared spectroscopic

The IR spectra were recorded with an FT-IR 8300 Shimadzu using pressed KBr discs and a spectral resolution of 4 cm^{-1}, and each spectrum was obtained after acquiring 98 spectra. FT-IR analyses were carried out with forsterite-91, forsterite-91 mixed with distilled water or artificial seawater. About 10 mg of samples plus 200 mg of KBr were weighed and ground in an agate mortar with a pestle until a homogeneous mixture was obtained. Disc pellets were prepared and spectra were recorded from 400 to 4000 cm^{-1}. FT-IR spectra were analysed by the Origin software (5.0, 2001).

Raman spectroscopy

Raman spectra were obtained from solid samples using a micro-Raman Spectrograph Renishaw in-Via with 633 nm laser line and 4 cm^{-1} resolution.

Electron paramagnetic resonance (EPR) spectroscopy

The samples were subjected to EPR experiment at an X-band (ca. 9 GHz) with 20 G modulation amplitude and magnetic field modulation of 100 kHz using a JEOL (JES-PE- 3X) spectrometer at room temperature. DPPH (2,2-difenil-1- picril-hidrazil) was used as g-marker and the standard of line intensity, using its spectral line ($g \approx 2.0036$).

Mössbauer spectroscopy

Mössbauer spectroscopy characterizations were performed in transmission geometry, using a conventional Mössbauer spectrometer, in a constant acceleration mode. The γ-rays were provided by a $^{57}Co(Rh)$ source, with initial nominal activity of 50 mCi. The Mössbauer spectra were analysed with a nonlinear least-square routine, with Lorentzian line shapes. All isomer shift (IS) data given are relative to α-Fe throughout this paper.

Table 2. *pH final, pH at point zero charge (pH_{PCZ}) and pH at isoelectric point (pH_{IEP})*

Sample	Environment	pH final[a]	pH_{PCZ}[b]	pH_{IEP}[c]
Forsterite-91	–		9.85	2.30
Forsterite-91, pH 1.9–2.2[d]	H_2O	6.7	9.40	3.60
	Artificial seawater	6.5	8.65	2.60
Forsterite-91, pH 8.0–8.4[d]	H_2O	9.0	9.59	2.72
	Artificial seawater	7.5	9.86	–

[a] pH after the samples were mixed for 24 hours.
[b] The pH_{PCZ} was measured as described by Uehara (1979).
[c] pH_{IEP} was measured as described in the Methods section.
[d] Initial range of pH of the solution.

X-ray diffractometry

The X-ray diffractograms were obtained in an XRD-6000 Shimadzu, using Cu Kα, a Ni monochromator, and the scanning parameters were set at 0.02°2θ, step width, count time 0.6 seconds and a measurement range from 2 to 30°2θ. The powder samples were placed on a glass slide. X-ray diffractograms were analysed by Grams/386 v 84.0 (Galactic Ind. Corp.) software.

Scanning electron microscopy (SEM)

SEM images were taken from SEM model Quanta 200 (FEI) Philips, in the laboratory of Scanning Electron Microscope and Microanalysis of UEL, equipped with an energy dispersive X-ray (EDX) model INCA 200 at 30 keV. The samples were fixed under 'stubs' in carbon adhesive tape and then coated with a layer of carbon or gold with 30 nm thickness.

Results and discussion

Table 2 shows the pH of the solution after forsterite-91 was mixed with distilled water and artificial seawater, as well as pH at point zero charge (pH_{PZC}) and pH at the isoelectric point (pH_{IEP}) (Fig. 1, zeta potential (ζ) versus pH). After mixing forsterite-91 samples in distilled water and artificial seawater at an initial pH 2.0 for 24 hours, we observed a large increase in the final pH of 6.7 and 6.5, respectively (Table 1). Charlou *et al.* (2002) measured the pH of Mid-Atlantic Ridge-MAR fluids and observed the following: pH = 2.8 (July 1997), pH = 2.5–3.0 (May 1998) and pH = 2.9 (May 2001). According to these data, the pH is approximately constant in the Atlantic Ridge-MAR which is likely due to the release of buffering compounds from the decomposition of orthopyroxene, which is more reactive than olivine. After the reactions with orthopyroxene are exhausted, the pH should increase. Thus, according to our results, the pH of hydrothermal vents should increase with increased dissolution of olivine.

Pokrovsky & Schott (2000a) suggested that these increases in pH are due to three reactions:

$$Mg_2SiO_{4(s)} + 4H^+_{(aq)} = 2Mg^{2+}_{(aq)} + H_4SiO_{4(aq)} \quad (1)$$

https://doi.org/10.1017/S147355041200050X Published online by Cambridge University Press

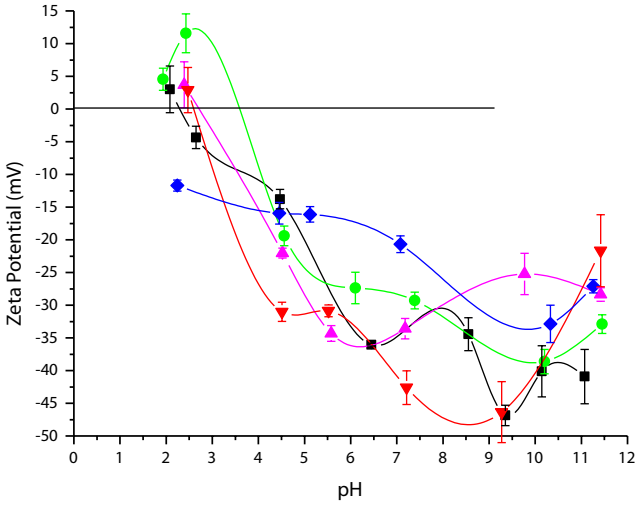

Fig. 1. Influence of pH on the zeta (ζ)-potential of solid forsterite-91 (------); forsterite-91 mixed with distilled water pH 2.0 (------) and pH 8.0 (------); forsterite-91 mixed with artificial seawater pH 2.0 (------) and pH 8.0 (------). All the samples were dissolved in a solution of 1 mmol L^{-1} KCl. And the pH was adjusted with 1.0 mol L^{-1} HCl or 1.0 mol L^{-1} NaOH.

$$> MgX + 2H^{+}_{(aq)} \leftrightarrow Mg^{2+}_{(aq)} + > 2HX \quad (2)$$

$$> 2HX + nH^{+}_{(aq)} = H_{n+2}X^{+} \quad (3)$$

Consumption of hydrogen from the solution would then be regulated by the formation of silicic acid (H_4SiO_4), and exchange reactions with Mg(II) adsorbed to the particles after dissolution. Furthermore, at low pH, protons are adsorbed by silanol and/or aluminol surface functional groups. For the samples mixed with distilled water and artificial seawater at pH 8.0 no large change in pH was observed (Table 2). Our results indicate that forsterite dissolution decreases rapidly at basic pH. This can be explained by equation (1), as the dissolution of forsteriteis favoured at lower pH. At basic pHs, the rates of forsterite dissolution are independent of pH (Pokrovsky & Schott 2000b). The increased dissolution of forsterite-91 at acidic pH release Fe(II) and could provide an explanation for the higher concentration of H_2 and CH_4 observed in Mid-Atlantic Ridge-MAR samples (Charlou *et al.* 2002). Gíslason & Arnórsson (1993) studied the dissolution of olivine in river water and cold groundwaters. They also observed a decrease in olivine dissolution at higher pHs.

Mass specific magnetic measurements (χ_{BF}) and magnification (×200) lenses of the original forsterite showed the presence of very small amounts of magnetite, which would be dissolved in acid pH, liberating not only Fe(II) but also Fe(III) to the solution. EPR spectra indicated that Fe(III) was present in the supernatant of forsterite-91 mixed with artificial seawater at pH 2.0, but was not observed in the experiment at basic pH (Fig. 2(c)). It should be noted that the concentration of Fe(III) is too low, because the Mössbauer spectra of all samples showed only doublets arising from Fe(II) (figure not shown). As magnetite in hydrothermal

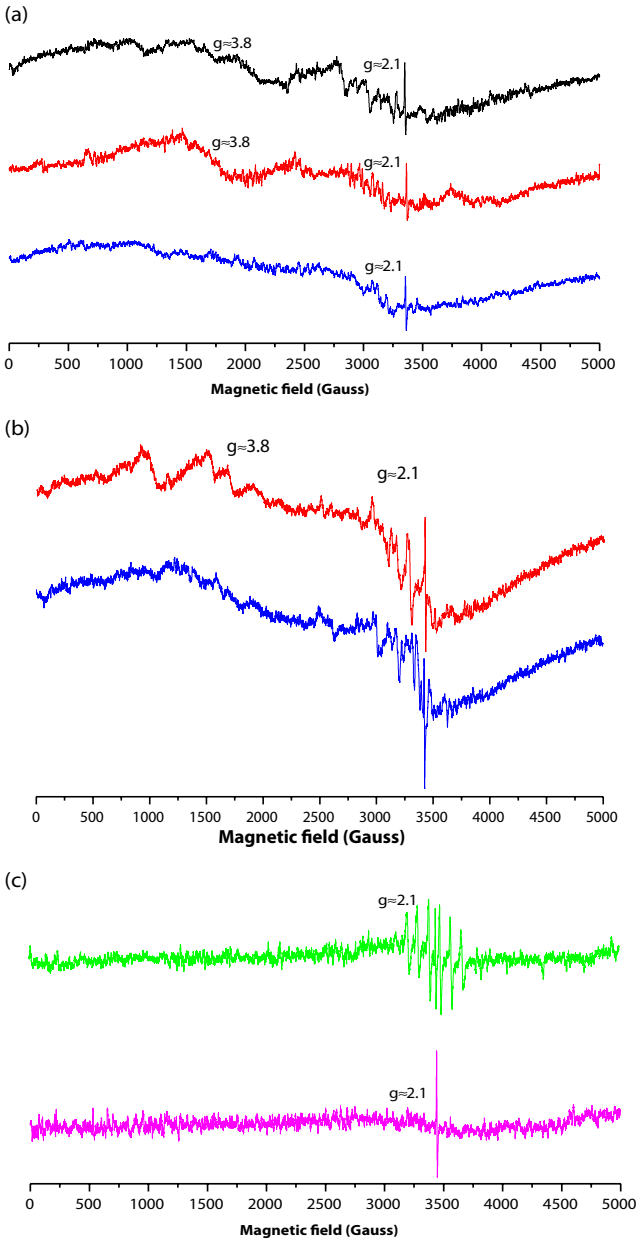

Fig. 2. EPR spectra: (a) solid forsterite-91 (------); forsterite-91 mixed with artificial seawater pH 2.0 (------) and forsterite-91 mixed with artificial seawater pH 8.0 (------); (b) forsterite-91 mixed with distilled water pH 2.0 (------) and forsterite-91 mixed with distilled water pH 8.0 (------); (c) supernatant of forsterite-91 mixed with artificial seawater pH 2.0 (------) and pH 8.0 (------). Forsterite-91 (100 mg) plus distilled water or artificial seawater (5.0 mL) was mixed for 24 hours.

environments at basic pH is a catalyst for reactions such as Fischer–Tropsch types, the lack of dissolution at this pH could favour synthesis of lipids that are essential for all forms of life (Neubeck *et al.* 2011). These results and SEM images (Fig. 3) show that the dissolution of forsterite-91 occurred at low pH.

For forsterite-91, the pH_{PZC} was 9.85 (Table 2); this value is in good agreement with those reported by Pokrovsky & Schott (2000a) (pH_{PZC} = 10) and Luce & Parks (1973) (pH_{PZC} = 8.9).

https://doi.org/10.1017/S147355041200050X Published online by Cambridge University Press

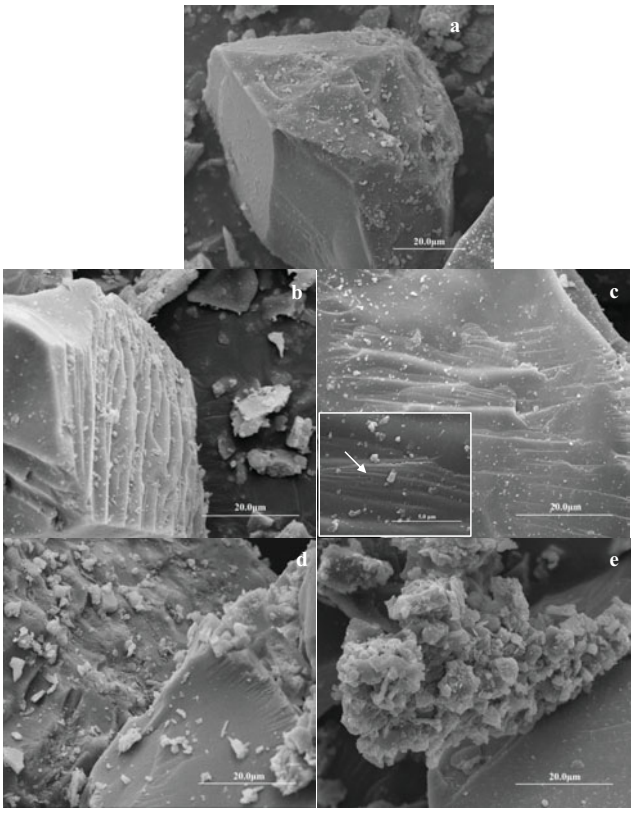

Fig. 3. SEM images of forsterite-91 samples: (a) forsterite-91; (b) forsterite-91 mixed with distilled water at pH 2.0; (c) forsterite-91 mixed with distilled water at pH 8.0; (d) forsterite-91 mixed with artificial seawater at pH 2.0 and (e) forsterite-91 mixed with artificial seawater at pH 8.0. With one exception forsterite-91 (a), all samples were mixed for 24 hours with distilled water or artificial seawater, after the solid was separated from supernatant by centrifugation (2000 rpm) and the solid as well as the supernatant were lyophilized.

In general, the treatments (distilled water and artificial seawater) decreased the pH_{PZC} of forsterite-91 (Table 2). Luce & Parks (1973) also observed a decrease in the pH_{PZC} of forsterite (pH_{PZC} 8.9) after weathering for 1 hour (pH_{PZC} 8.4) and 4 hours (pH_{PZC} 8.0). The decrease in pH_{PZC} values might be associated with the release of SiO_4^{4-} and the formation of an amorphous silicate phase on the surface of forsterite. Any adsorption or precipitation phase on the surface of forsterite-91 results in a decrease in the number of active sites on the mineral surface consequently affecting the rates of Fe(II) released into hydrothermal vent fluids (Béarat *et al.* 2006). Thus, the amount of magnetite, H_2, CH_4 and other substances may be similarly reduced (Hellevang *et al.* 2011). The pH_{IEP} of forsterite-91 was 2.3 (Table 2, Fig. 1). However, Pokrovsky & Schott (2000a), Deju & Bhappu (1966) and Ishido & Mizutami (1981) observed higher values of pH_{IEP} for olivine: 4.4 and 4.1 at 25 °C and 5.3 at 40 °C, respectively. Discrepancies among the pH_{PZC} and pH_{IEP} values also confirm the occurrence of dissolution/precipitation reactions of the olivine and other accessory minerals changing the surface properties of the mineral through the formation of different surface complexes. It also should be noted that the treatments (distilled water and artificial seawater) increased the pH_{IEP} of the samples (Table 2, Fig. 1). The trends of zeta potential versus pH were very different for untreated forsterite-91 samples and those treated with distilled water or artificial seawater (Fig. 1). This is an indication that the treatments changed the surface of forsterite-91 due to dissolution/precipitation reactions on the mineral surface. For both acidic and basic artificial seawater treatments, an increase in the zeta potential to pH ~6.0 was observed (Pokrovsky & Schott 2000a).

Figure 2 shows the EPR spectra of solid forsterite-91, forsterite-91 mixed with distilled water and artificial seawater as well as lyophilized supernatants of forsterite-91 mixed with artificial seawater. The spectrum of solid forsterite-91 exhibits two resonance lines at $g \approx 2.1$ and at $g \approx 3.8$ (Fig. 2(a)). The resonance line at $g \approx 2.1$ represents the characteristic signal of Fe(III) in octahedral coordination sites; here, it is associated with spin–spin interactions in the surface and there is the cubic symmetry being interstitially more available and active. The line $g \approx 3.8$ can be ascribed to high-spin Fe(III) ions held in the inner-sphere in octahedral sites with rhombic symmetry (Guskos *et al.* 2002; Carbone *et al.* 2005; Mota *et al.* 2009). These lines were also observed in forsterite-91 samples after mixing with distilled water and artificial seawater at pH 2.0 (Fig. 2(a) and (b)). The line at $g \approx 2.1$ was only observed for the sample of forsterite-91 mixed with distilled water and artificial seawater at pH 8.0 and supernatants (Fig. 2(a–c)). Talik *et al.* (2006) reported that synthetic forsterite crystals did not give any EPR spectra because, for this mineral, Fe(II) is present and this line is observable by EPR only at very low temperatures (< 5 K). Our samples showed the presence of Fe(III) associated with the presence of magnetite particles and Fe(II) oxidized to Fe(III) from the dissolution of minerals. Using similar reasoning, Sugimori *et al.* (2012) observed that some Fe(II) that were released from olivine were oxidized and precipitated as Fe(III) oxides/hydroxides. The presence of iron oxides (magnetite) in forsterite-91 samples after mixing with artificial seawater or distilled water, even in small amounts, is an important result because these substances are catalysts for the formation of CH_4 in hydrothermal vents (Charlou *et al.* 2002; Martin *et al.* 2008; Neubeck *et al.* 2011). However, after grinding and subjecting the sample to chemical treatments, SEM images or X-ray diffraction (XRD) patterns of our samples did not appear to contain oxides/hydroxides (Figs. 3 and 5). In addition, analysis of the original forterite-91 sample showed Mn (Table 1), and the characteristics line for Mn(II) was only observed in the EPR spectra of the lyophilized supernatant after forsterite-91 was mixed with artificial seawater at pH 2.0 (Fig. 2(c)). Manganese–Mn was detected in acidic hydrothermal vents in concentrations up to 2250 μM (Charlou *et al.* 2002). It should be noted that Mn is a catalyst in FTT reactions that are very common in hydrothermal vents (Charlou *et al.* 2002; Lohitharn & Goodwin Jr. 2008). Mn in our samples was probably not divalent, but in a higher oxidation state with low intensity, or the intensity of the Fe(III) signal was much bigger than that of Mn (Table 1). Talik *et al.* (2006) obtained the characteristic signal of Mn(II) for all natural samples of olivine when analysed at 90 K. All the

https://doi.org/10.1017/S147355041200050X Published online by Cambridge University Press

Table 3. *Elements composition of forsterite-91 samples using SEM–EDS*

Samples	pH	Samples phase[a]	Elements													
			Si	O	Mg	Fe	Mn	Al	Ni	Na	Cr	Cl	S	Ca	Br	K
Forsterite-91	–	So	+	+	+	+	+	+	+	–	+	–	–	+	–	+
Forsterite-91 plus distilled water	2.0	So	+	+	+	+	–	+	+	–	+	–	–	–	–	–
		Su	+	+	+	+	–	–	+	+	–	+	–	–	–	–
	8.0	So	+	+	+	+	–	+	+	–	+	–	–	–	–	–
		Su	+	+	+	+	–	+	–	–	–	+	–	+	–	+
Forsterite-91 plus seawater	2.0	So	+	+	+	+	+	+	+	+	–	+	+	–	+	–
		Su	+	+	+	–	–	+	–	+	–	+	+	+	–	+
	8.0	So	+	+	+	+	+	+	+	+	+	+	+	+	–	+
		Su	+	+	+	–	–	+	–	+	–	+	+	+	–	+

[a] Samples phase: so = solid and su = supernatant.

results shown above indicate that Mn(II) and Fe(III) are present at low concentrations as contaminants.

Figure 3 shows SEM images of forsterite-91 and forsterite-91 mixed with distilled water and artificial seawater. SEM images of all samples showed etch pits only for forsterite-91 sample mixed with distilled water at pH 8.0 (Fig. 3(c), insert). However, etch pits were also observed in the weathered natural olivine (Velbel 2009), as well as in dissolution experiments with forsterite-91 (Pokrovsky & Schott 2000b). SEM images also showed the characteristic cubic shape of halite in the samples of forsterite-91 mixed with artificial seawater (Fig. 3(d) and (e)); this result was also confirmed by X-ray diffractometry (Fig. 5). Daval *et al.* (2011) studied the effect of CO_2 and NaCl on the dissolution of the olivine and also observed the presence of halite in SEM images. The precipitation of halite on forsterite-91 could decrease the release of Fe(II) and consequently the synthesis of magnetite, which is a catalyst for the formation of lipids in hydrothermal vents (Charlou *et al.* 2002; Martin *et al.* 2008; Neubeck *et al.* 2011).

Table 3 shows the microanalysis of several elements using SEM-EDS. The microanalysis of the samples of forsterite-91 mixed with artificial seawater (both solid and supernatant) showed the presence of Na, Cl, S, Ca and K, which could be due to the artificial seawater that was used in the experiments or contaminants from the original sample (Table 1). The elements Si, Mg, Fe and Al were detected in almost all supernatant samples. This was due to forsterite-91 dissolution, which can be confirmed by the SEM images (Fig. 3) (Pokrovsky & Schott 2000a). These elements were also found in hydrothermal vents due to the dissolution of minerals (Charlou *et al.* 2002; Valsami-Jones *et al.* 2005). Chromium was detected in almost all solids, but it was not detected in any supernatant (Table 3). Valsami-Jones *et al.* (2005) studied the hydrothermal vents system of Milos island and Hellenic Volcanic Arc. According to these authors, the concentration of chromium was enriched (3.0 μM) only in one sample and was not detected in most of the other samples. Foustoukos & Seyfried Jr (2004) studied the synthesis of hydrocarbons under hydrothermal vents conditions and showed that Cr_2O_3 in combination with iron oxide was a catalyst for FTT synthesis of hydrocarbons. The low concentration of chromium in hydrothermal vents and lack of dissolution of minerals with chromium in our experiments could be an indication that this catalyst would be active in these environments.

The FT-IR spectrum of forsterite-91 showed a broad band at 3439 cm^{-1} and another weak band at 3679 cm^{-1}. The band at 3439 cm^{-1} could be attributed to OH from the hydration of forsterite-91 (Yang & Keppler 2011) or to the hydration of several trivalent cations (Fe, Mn and Cr) present in forsterite-91 (Berry *et al.* 2007). The band at 3439 cm^{-1} could also be due to Fe(III) which was observed in EPR spectra (Fig. 2) and in the original sample (magnetite) before grinding. It could also be due to Cr(III) or Mn(III), as Mn was found in the original sample (Table 1) and Cr was observed in the microanalysis using SEM-EDS (Table 3). The band at 3679 cm^{-1} can be ascribed to OH in zeolites (Jacobs & Uytterhoeven 1973). It should be noted that this band vanished after the treatment with artificial seawater, probably due to the dissolution of zeolite (Fig. 5). The FT-IR spectrum of forsterite-91 also showed bands at 470, 506, 608 cm^{-1} and 839, 887, 955, 987 cm^{-1} that could be attributed to Si–O bending and Si–O asymmetric stretching, respectively (figure not shown) (Hamilton 2010). These bands did not change after forsterite-91 was mixed with distilled water or artificial seawater (figure not shown).

Figure 4 shows Raman spectra of forsterite-91 and the samples of forsterite-91 mixed with distilled water and artificial seawater. The Raman spectrum of forsterite-91 showed two bands at 822 and 854 cm^{-1} which are attributed to asymmetric SiO_4 stretching (Kolesov & Geiger 2004; Kuebler *et al.*, 2006). Figure 4 also shows small bands in the 500–700 cm^{-1} spectral region resulting from internal bending vibrational modes of the SiO_4 ionic groups (Kuebler *et al.*, 2006). However, these bands are too small for any identification. According to Kuebler *et al.* (2006), the ratios of Mg/(Mg + Fe) in olivine samples determines the shifting of these bands. When this ratio increased, the peak position of the band shifted to higher wavenumbers (Kuebler *et al.*, 2006). A small shift was observed for the sample of forsterite-91 mixed with distilled water at pH 2.0 (Fig. 4). The micro-analysis by SEM-EDS showed Fe and Mg in the supernatant of this sample (Table 3). In addition, EPR spectra showed Fe(III) in

https://doi.org/10.1017/S147355041200050X Published online by Cambridge University Press

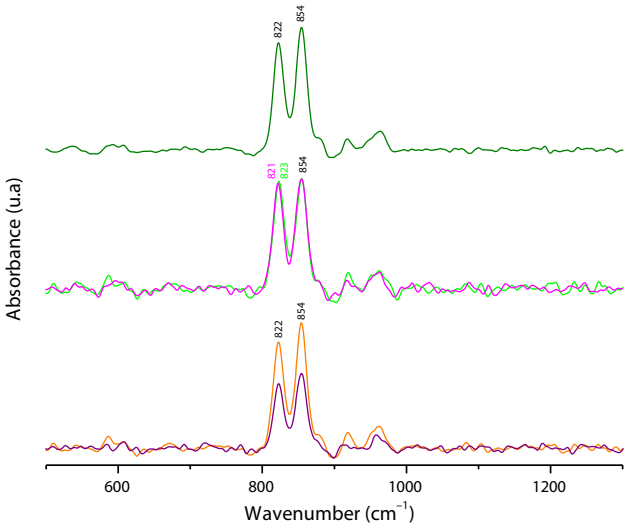

Fig. 4. Raman spectra of the samples: forsterite-91 without previous treatment (------); forsterite-91 mixed with disttiled water at pH = 2.0 (------) and pH = 8.0 (------); forsterite-91 mixed with artificial seawater at pH = 2.0 (------) and pH = 8.0 (------). All the samples of forsterite-91 (100 mg) plus distilled water or artificial seawater, (5.00 mL) were mixed for 24 hours, centrifuged, separated from the supernatants and lyophilized.

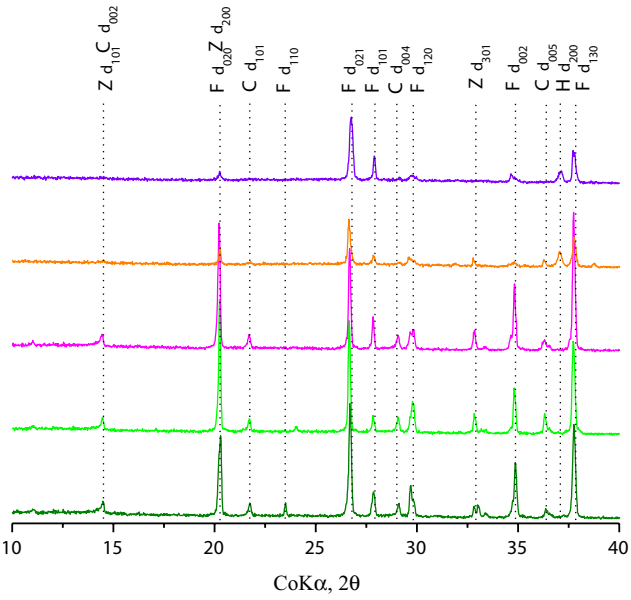

Fig. 5. X-ray diffractogram of the samples: forsterite-91 without previous treatment (------); forsterite-91 plus distilled water at pH = 2.0 (------) and pH = 8.0 (------) and forsterite-91 plus artificial seawater at pH = 2.0 (------) and pH = 8.0 (------). All the samples of forsterite-91 (100 mg) plus solutions, distilled water or artificial seawater, (5.00 mL) were mixed for 24 hours, centrifuged, separated from the supernatants and lyophilized. Z = zeolite; F = forsterite-91; C = clinochlore; H = halite.

the supernatant of the samples of forsterite-91 mixed with artificial seawater (Fig. 2(b)); the Raman spectra did not show any shift of the bands at 822 and 854 cm^{-1} (Fig. 4).

The XRD patterns of forsterite-91 shown in Fig. 5 indicate that the samples are almost pure, but small diffraction peaks of clinochlore and zeolite were observed, representing less than 5% of the sample. Smaller concentrations of magnetite (Fe_3O_4) were also observed in the original sample, before grinding by a ×200 magnification lens. However, the diffractograms of the samples of forsterite-91 mixed with artificial seawater showed the total dissolution of the zeolites at both acidic and basic pH (2.0 and 8.0). Baú *et al.* (2012) also observed that artificial seawater had a major effect on the dissolution of zeolites. Synthetic zeolites have also been used in experiments investigating peptide synthesis in hydrothermal vents (Zamaraev *et al.* 1997). Experiments should be undertaken to verify which natural zeolites could not be dissolved by seawater. As suggested previously, it is important to use synthetic as well as natural materials for these investigations (Zaia 2012). In the seawater treatment, the presence of halite (NaCl) was also observed as a residual mineral after processing the samples (Fig. 5). This result was also confirmed by SEM images (Fig. 3). The treatments of the powder minerals in distilled water at different pHs (2.0 and 8.0) indicate the partial dissolution of zeolite. The treatment of the powder material with distilled water had no influence on the XRD patterns of forsterite-91. Excluding the dissolution of the zeolite and partial dissolution of clinochlore, the treatment of forsterite-91 with artificial seawater decreased the intensity of most diffraction peaks, indicating significant dissolution of the mineral (Figs. 3 and 5). The dissolution process of olivine could have resulted from the presence of anions or the hydronium ion (Rosso & Rimstidt 2000) in artificial seawater or the low content of Mg in artificial seawater which is undersaturated with respect to forsterite (Gíslason & Arnósson 1993).

Conclusion

The dissolution of forsterite-91 in distilled water or artificial seawater at initial pH 2.0, resulted in an increase in pH. This result could mean that, in hydrothermal vents, the release of more Fe(II) could result in an increase in the amount of hydrocarbons and magnetite. In general, the treatments with distilled water or artificial seawater decreased the pH_{PZC} and increased the pH_{IEP} of the forsterite-91. The ions of artificial seawater affected the zeta potential. These effects occurred due to adsorption/precipitation of substances on the surface of forsterite-91.

The EPR spectra showed the presence of Fe(III); however, the concentration was likely low, as Mössbauer spectra showed only a doublet due to Fe(II). The presence of Fe(III) is an indication of magnetite, which may serve as a catalyst in hydrothermal vents. The microanalysis of forsterite-91 showed the presence of Mn, but its oxidation could be other than +II, as this signal was only detected in EPR spectra of supernatant samples after mixing with artificial seawater at pH 2.0. The release of Mn(II) is important, because this metal may also serve as a catalyst in hydrothermal vents.

SEM images showed etch pits only in the sample of forsterite-91 mixed with distilled water at pH 8.0. For the samples of forsterite-91 mixed with artificial seawater, SEM

https://doi.org/10.1017/S147355041200050X Published online by Cambridge University Press

images also showed the characteristic cubic shape of halite. The presence of halite on the surface of the mineral could decrease the release of Fe(II) into solution and consequently, in hydrothermal vents systems decrease the amount of hydrocarbons synthesized.

SEM-EDS analysis of the samples mixed with artificial seawater showed the following elements Na, Cl, S, Ca and K, which may have been contributed by artificial seawater used in the experiments or contaminants from the original sample. The elements Si, Mg, Fe and Al were detected in almost all supernatant samples, due to dissolution of the samples. Cr was not detected in any supernatant, meaning that it could remain in the solid phase to catalyse reactions in hydrothermal vents.

FT-IR spectra of the forsterite-91 mixed with artificial seawater showed that the band at 3679 cm^{-1}, due to OH in zeolites vanished because of their total dissolution. Synthetic zeolites have been used for synthesis of peptides in experiments simulating hydrothermal vents; however, experiments with natural zeolites should also be performed. Raman spectra of the forsterite-91 with and without any previous treatments did not show any difference.

X-ray diffractograms of the original forsterite-91 showed small peaks due to zeolites and clinochlore. A very small concentration of magnetite was also observed in the original sample, before grinding with a magnification lens (×200). X-ray diffractograms showed dissolution of zeolite and a small peak due to halite, after the samples were treated with artificial seawater. A strong dissolution process of the sample of forsterite-91 was observed after treatment with artificial seawater.

Acknowledgments

J.P.T.B. and C.M.D.S./C.E.A.C. acknowledge the fellowships from PIBIC/CNPq/UEL and Capes, respectively. The authors thank Dr Luis Otávio B Benetoli (UFSC) for zeta potential determinations and to Dra. Célia GTJ Andrade (Microscopy and Microanalysis Lab, UEL) for SEM-EDS analysis. This research was supported by grants from CNPq (474985/2010-5) and Fundação Araucária (15279/2009).

References

Baú, J.P.T. *et al.* (2012). Adsorption of adenine and thymine on zeolites: FT-IR and EPR spectroscopy and X-ray diffractometry and SEM studies. *Orig. Life Evol. Biosph.* **42**, 19–29.

Béarat, H., Mckelvy, M.J., Chizmeshya, A.G., Gormley, D., Nunez, R., Carpenter, R.W., Squires, K. & Wolf, G.H. (2006). Carbon sequestration via aqueous olivine mineral carbonation: role of passivating layer formation. *Environ. Sci. Technol.* **40**, 4802–4808.

Berry, A.J., O'Neill, H.St.C., Hermann, J. & Scott, D.R. (2007). The infrared signature of water associated with trivalent cations in olivine. *Earth Planet. Sci. Lett.* **261**, 134–142.

Brown, E., Colling, A., Park, D., Phillips, J., Rothery, D. & Wright, J. (2004). *Seawater: Its Composition, Properties and Behavior*. The Open University, Oxford.

Carbone, C., di Benedetto, F., Marescotti, P., Sangregorio, C., Sorace, L., Lima, N., Romanelli, M., Luchetti, G. & Cipriani, C. (2005). Natural Fe-oxide and -oxyhydroxide nanoparticles: an EPR and SQUID investigation. *Miner. Petrol* **85**, 19–32.

Charlou, J.L., Donval, J.P., Fouquet, Y., Jean-Baptiste, P. & Holm, N.G. (2002). Geochemistry of high H_2 and CH_4 vent fluids issuing from ultramafic rocks at the rainbow hydrothermal field (36°14′N, MAR). *Chem. Geol.* **191**, 345–359.

Daval, D. *et al.* (2011). Influence of amorphous silica layer formation on the dissolution rate of olivine at 90 °C and elevated pCO_2. *Chem. Geol.* **284**, 193–209.

Deju, R.A. & Bhappu, R.B. (1966). A chemical interpretation of surface phenomena in silicate minerals. *Trans. A.I.M.E.* **235**, 329–332.

Foustoukos, D.I. & Seyfried, W.E. Jr. (2004). Hydrocarbons in hydrothermal vent fluids: the role of chromium-bearing catalysts. *Science* **304**, 1002–1005.

Giammar, D.E., Bruant, R.G. Jr. & Peters, C.A. (2005). Forsterite dissolution and magnesite precipitation at conditions relevant for deep saline aquifer storage and sequestration of carbon dioxide. *Chem. Geol.* **217**, 257–276.

Gíslason, S.R. & Arnórsson, S. (1993). Dissolution of primary basaltic minerals in natural waters: saturation state and kinetics. *Chem. Geol.* 105, 117–135.

Guskos, N. *et al.* (2002). Photoacoustic, EPR and electrical conductivity investigations of three synthetic mineral pigments: hematite, goethite and magnetite. *Mater. Res. Bull.* **37**, 1051–1106.

Hamilton, V.E. (2010). Thermal infrared (vibrational) spectroscopy of Mg–Fe olivines: a review and applications to determining the composition of planetary surfaces. *Chem. Erde* **70**, 7–33.

Hazen, R.M., Papineau, D., Bleeker, W., Downs, R.T., Ferry, J.M., McCoy, T.J., Sverjensky, D.A. & Yang, H. (2008). Mineral evolution. *Am. Miner.* **93**, 1693–1728.

Hellevang, H. (2008). On the forcing mechanism for the H_2-driven deep biosphere. *Int. J. Astrobiol.* **7**, 157–167.

Hellevang, H., Huang, S. & Thorseth, I.H. (2011). The potential for low-temperature abiotic hydrogen generation and a hydrogen-driven deep biosphere. *Astrobiology* **11**, 711–724.

Ishido, T. & Mizutani, H. (1981). Experimental and theoretical basis of electrokinetic phenomena in rock-water system and its application to geophysics. *J. Geophys. Res.* **86**, 1763–1775.

Jacobs, P.A. & Uytterhoeven, J.B. (1973). Assignment of the hydroxyl bands in the infrared spectra of zeolites X and Y Part 1 Na-H zeolites. *J. Chem. Soc. Faraday Trans. I.* **69**, 359–372.

King, R.J. (2009). Minerals explained 50: olivine group. *Geol. Today* **25**, 193–197.

Kolesov, B.A. & Geiger, C.A. (2004). A Raman spectroscopy study of Fe-Mg olivines. *Phys. Chem. Miner.* **31**, 142–154.

Kuebler, K.E., Jolliff, B.L., Wang, A. & Haskin, L.A. (2006). Extracting olivine (Fo–Fa) compositions from Raman spectral peak positions. *Geochim. Cosmochim. Acta* **70**, 6201–6222.

Lohitharn, N. & Goodwin, J.G. Jr. (2008). Impact of Cr, Mn and Zr addition on Fe Fischer–Tropsch synthesis catalysis: investigation at the active site level using SSITKA. *J. Catal.* **257**, 142–151.

Luce, R.W. & Parks, G.A. (1973). Point of zero charge of weathered forsterite. *Chem. Geol.* **12**, 147–153.

Martin, W., Baross, J., Kelley, D. & Russell, M.J. (2008). Hydrothermal vents and the origin of life. *Nat. Rev. Microbiol.* **6**, 805–814.

Mormile, M.R., Hong, B.Y., & Benison, K.C. (2009). Molecular analysis of the microbial communities of Mars analog lakes in Western Australia. *Astrobiology* **9**, 919–930.

Mota, L., Toledo, R., Faria, R.T. Jr., da Silva, E.C., Vargas, H. & Deladillo-Hotfort, I. (2009). Thermally treated soil clays as ceramic raw materials: characterization by X-ray diffraction, photoacoustic spectroscopy and electron spin resonance. *Appl. Clay Sci.* **43**, 243–247.

Nahon, D., Colin, F. & Tardy, Y. (1982). Formation and distribution of Mg, Fe, Mn-smectites in the first stages of lateritic weathering of forsterite and tephroite. *Clays Miner.* **17**, 339–48.

Neubeck, A., Duc, N.T., Bastviken, D., Crill, P. & Holm, N.G. (2011). Formation of H_2 and CH_4 by weathering of olivine at temperatures between 30 and 70 °C. *Geochem. Trans*. **12**, 6.

Olsen, A.A. & Rimstidt, J.D. (2008). Oxalate-promoted forsterite dissolution at low pH. *Geochim. Cosmochim. Acta* **72**, 1758–1766.

Pokrovsky, O.S. & Schott, J. (2000a). Forsterite surface composition in aqueous solutions: a combined potentiometric, electrokinetic, and spectroscopic approach. *Geochim. Cosmochim. Acta* **64**, 3299–3312.

Pokrovsky, O.S. & Schott, J. (2000b). Kinetics and mechanism of forsterite dissolution at 25 °C and pH from 1 to 12. *Geochim. Cosmochim. Acta* **64**, 3313–3325.

Rosso, J.J. & Rimstidt, J.D. (2000). A high resolution study of forsterite dissolution rates Geochim. *Geochim. Cosmochim. Acta* **64**, 797–811.

Stopar, J.D., Taylor, G.J., Hamilton, V.E. & Browning, L. (2006). Kinetic model of olivine dissolution and extent of aqueous alteration on Mars. *Geochim. Cosmochim. Acta* **70**, 6136–6152.

Sugimori, H., Kanzaki, Y. & Murakami, T. (2012). Relationships between Fe redistribution and PO_2 during mineral dissolution under low O_2 conditions. *Geochim. Cosmochim. Acta* **84**, 29–46.

Talik, E., Zarek, W., Kruczek, M., Ganschow, S., Skrzypek, D. & Popiel, E. (2006). Characterization of olivine single crystals grown by the micropulling down method and terrestrial olivine by XPS, Mössbauer, magnetic and EPR methods. *Cryst. Res. Technol*. **41**, 979–987.

Uehara, G. (1979). Mineral–chemical properties of oxisols. In *International Soil Classification Workshop*, Soil Survey Division Land Development Department, Bangkok, Malaysia, vol. 2, pp. 45–60.

Valsami-Jones, E., Baltatzis, E., Bailey, E.H., Boyce, A.J., Alexander, J.L., Magganas, A., Anderson, L., Waldron, S. & Ragnarsdottir, K.V. (2005). The geochemistry of fluids from an active shallow submarine hydrothermal system: Milos island, Hellenic Volcanic Arc. *J. Volcanol. Geotherm. Res*. **148**, 130–151.

Velbel, M.A. (2009). Dissolution of olivine during natural weathering. *Geochim. Cosmochim. Acta* **73**, 6098–6113.

Yang, X.Z. & KeppLer, H. (2011). *In situ* infrared spectra of OH in olivine to 1100 °C. *Am. Mineral*. **96**, 451–454.

Zaia, D.A.M. (2012). Adsorption of amino acids and nucleic acid bases onto minerals: a few suggestions for prebiotic chemistry experiments. *Int J. Astrobiol*. **11**, 229–234.

Zamaraev, K.I., Romannikov, V.N., Salganik, R.I., Wlassoff, W.A. & Khramtsov, V.V. (1997). Modelling of the prebiotic synthesis of oligopeptides: silicate catalysts help to overcome the critical stage. *Orig. Life Evol. Biosph*. **27**, 325–337.

https://doi.org/10.1017/S147355041200050X Published online by Cambridge University Press